A Method for Thoracic Injury Risk Function Development for Human Body Models

Jason Forman, Shubham Kulkarni, Daniel Perez-Rapela, Sayak Mukherjee,
Matthew Panzer, Jason Hallman

Abstract This study describes a method to tune stochastic strain-based thoracic injury risk functions (IRFs) for specific human body models, illustrated using THUMS v.4.1 and GHBMC v.6.0. One hundred and seventy simulations were performed for each model in thirteen frontal-impact loading modes derived from tests on postmortem human surrogates (PMHS) reported in the literature. These included hub-impact tests, bar impact tests, and table-top tests with belt and distributed loading. Local strain-based IRFs were then optimised to result in the best fit compared to the injury outcomes observed in the PMHS tests. The resulting IRFs were then examined in selected whole-body simulations (in sled and vehicle environments) to evaluate their general predictive capability. The results suggested that direct application of rib cortical bone ultimate strain data to the THUMS v4.1 would result in underestimation of rib fracture risk compared to the reference PMHS tests. Tuning the local strain IRFs for each model, however, tended to result in reasonable injury risk prediction compared to PMHS tests and compared to risks derived from field data. Through tuning the local strain IRFs for application to a specific HBM, this framework provides a means to arrive at comparable injury risk prediction across HBMs of differing construction.

Keywords Human body model, injury risk function, rib fracture, simulation, thorax.

I. INTRODUCTION

In recent years, finite element human body models (FE-HBMs or HBMs) have been developed as research tools for restraint systems and injury prediction in simulations. However, for HBMs to be fully useful as a virtual assessment tool, standardised methods are needed for translating the outputs from HBM simulations into predicted risk of injury. An important body region of interest for such standardisation is the thorax. The thorax was one of the first body regions for which anatomical structures were modelled in detail in HBMs [1-3], and the thorax remains one of the most frequently injured body regions in motor vehicle collisions (MVCs) [4-6].

Unlike physical occupant models, i.e., dummies, HBMs provide the potential to predict injury based on distributed internal measures such as stress or strain. By removing constraints inherent to measurement with physical instrumentation, strain-based prediction with HBMs may be less prone to artificial sensitivity to the location or pattern of load application. Despite this advantage, the challenge with strain-based ribcage injury prediction lies in the question of how to interpret strain information across the entirety of the ribcage to predict the probability (risk) of incurring a specific number of rib fractures to assess overall injury severity, i.e., to classify based on Abbreviated Injury Scale (AIS) definitions of rib fracture severity [7]). Drawing from past work in probabilistic system failure analysis, [8] described an approach to combine rib fracture probabilities calculated throughout the rib cage into an aggregated risk assessment targetting a selected injury severity level. Using this method, one can predict the risk of a selected number of fractures, e.g., 3+ fractures, 7+ fractures, etc., based on the collection of maximum principal strains output from a HBM's ribs. As the local risk is translated into a whole-ribcage risk by combining the risks predicted for each rib, the risk of a specific injury severity may be calculated using a single local strain injury risk function (IRF). This method has been used in various exploratory studies investigating potential application with different HBMs [9-10], and has been refined by populating with expanded datasets on local failure properties of rib cortical bone [11].

Even with strain-based methods, however, it is possible that different local IRFs may be needed for comparable injury prediction with different HBMs. The strain measured in the ribs of HBMs is not just a matter of the HBM's gross biofidelity – it can also be dependent on the subtle modelling characteristics employed in the

J. Forman is a Principal Scientist at the University of Virginia Center for Applied Biomechanics in Charlottesville, Virginia, USA (phone: +1-434-297-8051; e-mail: jlf3m@virginia.edu). S. Kulkarni is a M.Sc. student, Daniel Perez-Rapela is a Research Scientist, Sayak Mukherjee is a Ph.D. student, and Matthew Panzer is an Associate Professor in the Department of Mechanical and Aerospace Engineering at the University of Virginia, USA. Jason Hallman is a Senior Manager at Toyota Motor North America, USA.

HBM (for example, mesh size). In addition, substantial variability exists in the PMHS reference data for assessing a model's strain-level biofidelity [12]. With PMHS strain biofidelity corridors often exhibiting a 200% or greater range of variability, two HBMs could both be judged as reasonably biofidelic (by falling within the PMHS strain corridors) while still exhibiting substantially different strains from eachother. Thus, even for two HBMs of comparable biofidelity, different local strain IRFs may be needed to arrive at similar injury prediction between the two models when evaluated in matched loading scenarios. One could try to harmonise injury prediction by continuing to modify their HBM to arrive at the same strain magnitudes in the ribs as observed in other models. This may not be necessary, however, if local strain IRFs can be tuned for specific HBMs, based on the strain magnitudes that they naturally experience in their ribs. This study seeks to develop a framework to do just that – to tune local strain IRFs for rib fracture injury prediction in HBMs of differing construction, based on rib strains observed in a large set of simulations in selected reference conditions. This framework is intended to be applicable for tuning a local strain IRF for any HBM. This framework was first developed and illustrated using the THUMS v4.1 HBM, and then was applied to the GHBMC v.6.0 HBM to investigate if a different strain IRF would be needed to arrive at comparable injury risk prediction between the two models. As is common with other types of IRF development efforts, this IRF development framework was based on performing simulations seeking to match test conditions used in previous reference tests with post-mortem human surrogates (PMHS) and then optimising the IRFs to best fit the injury outcomes observed in those tests. The tuned local IRFs were then applied in selected whole-body simulation scenarios to examine the general predictive ability of the resulting functions/models.

II. METHODS

Loadcases & Simulation Strategies

The literature was reviewed to identify past PMHS tests involving frontal thoracic loading that may be used as load cases to perform matched simulations for IRF tuning. The basic selection criteria were:

- The test series must involve frontal loading of an intact thorax, i.e., no denuded or eviscerated tests
- The test conditions and loading environment must be described with sufficient detail to reproduce in simulation with reasonable confidence
- Injuries are described for each test subject
- When the loading input varied by test, e.g., impactor mass or velocity, or belt displacement input, the specific loading input must be described for each test

This search resulted in 13 load cases described in 17 studies [13-29], comprised of various impactor test series and test series using a table-top device to compress the chest using different types of load application (hub, diagonal belt, etc.). In total, these impactor and table-top studies included 170 PMHS tests (some of which were repeated tests performed on the same PMHS). The basic details of these test series are included in Table I.

For each loadcase listed in Table I, simulations were set up based on information included in the published studies. Brief information on each loadcase setup is included in Appendix A (and more detailed information is available on request). In some cases, there is overlap with loadcases that are included in the publicly available validation suite for THUMS v4.1. For those, the publicly available validation environment setups were used directly for this study.

The collection of loadcases included five impactor-style test series. This included tests with a hub-style circular impactor impacting in either the mid-sagittal plane [13-15] or at an oblique orientation [16]. Other impactor-style cases included rigid bar impact to the lower ribcage [17], and tests with an impactor shaped like a steering-wheel rim [18]. All cases except the steering wheel rim impact were performed in a free-back condition, where the PMHS thoraces were free to move rearward during the impact. In those cases, the simulations were driven simply by defining the mass and initial velocity of the impactor. The steering wheel rim impact [18] was performed in a rigid-back condition, where the spine was affixed to a rigid bar. That case used a stroke-limited impactor with a large mass (to minimise inertial loss), which was also applied in the simulations.

After setting up the impactor loadcases, one simulation was performed for each individual PMHS test. For each of these test-specific simulations, the impactor initial velocity was defined based on the impactor initial velocity for the target *matched* PMHS test. The impactor mass for each simulation was also initially set to target the impactor mass used in each matched PMHS test. To provide some accounting for differences in the size of the PMHS, however, the impactor mass for each simulation was scaled by the PMHS mass in the targeted

matched test. This ensured that the relative momentum of the impactor and PMHS remained constant between the PMHS tests and the matching simulations. The impactor velocities, masses, and scaled masses for each impactor simulation are listed in Appendix C.

In addition to the impactor loadcases, the dataset used here also included eight test series using table-top style loading, where a PMHS thorax is place supine on a rigid table outfitted with a specific type of loader (belt, hub, etc.) which then is used to compress the thorax against the table [19]. The loader types present in this dataset included a hub-type loader, a single diagonal belt (similar in position to a shoulder belt), a double diagonal belt, i.e., bilateral symmetric shoulder belts, and a large distributed belt arranged horizontally across the chest to apply a distributed load without engaging the shoulders. The test series of [20] also used a double-diagonal belt arrangement where different tensions were applied in the left and right shoulder belt (accomplished via differential force limiters). In some test series [19-20], the posterior aspect of the thorax was supported simply by laying on the tabletop, allowing some degree of flexibility in the spine during the test. In other cases [21-22], the spine was rigidly affixed to a sturdy posterior support. These boundary conditions were replicated in the simulations. In most cases, the tabletop PMHS tests were controlled via a prescribed displacement applied to the loading device, i.e., via a prescribed displacement applied to the ends of the loading belt. This strategy was also employed in the simulations. For each simulation, the displacement time-history of the loading device was prescribed, based on the displacement time-history reported for each target matched PMHS test. To account for differences in PMHS chest size, this displacement time history was scaled (in magnitude) based on the chest depth of the PMHS (relative to the THUMS model). Thus, for each simulation the prescribed displacement was defined to target the % chest compression applied in each matching PMHS test. (Note: This strategy was slightly modified for the case of [23-24] where the loader motion was defined based on its velocity time history, which was also scaled in magnitude by the target PMHS's chest depth.) Most of the table-top cases included repeated tests performed on individual PMHSs with an initial low compression magnitude, followed by a final test of a high compression magnitude. In those cases, it was assumed that the injuries that were observed occurred during the high-severity tests, and that the low-severity tests were non-injurious.

As described below, the impactor and table-top cases were used to tune a thoracic injury prediction method for application to THUMS v4.1. We then sought to check the reasonableness of its predictive ability using an independent dataset not included in the IRF fitting. For this, we performed simulations based on several PMHS sled test series, targeting cases that represent a range of loading severities and injury outcomes. This included the 30 km/h and 40 km/h *Gold Standard* tests reported by [25] and [26], comprised of a simplified loading environment designed to isolate loading of the chest by a seatbelt with various loading severities (with a rigid seat, rigid knee bolster, and either standard or force-limited 3-point belt). In addition, simulations were performed based on the rear seat frontal-impact sled tests reported by [27] and [28]. These were all performed at an impact velocity of 48 km/h, and included tests with a standard 3-point belt and tests with a 3-point belt with a retractor pretensioner and a progressive force limiter. Simulations were also performed based on the 29 km/h right-front-passenger tests of [298], which included restraint by a standard (not force limited or pretensioned) belt. A single simulation was performed for each sled test series, seeking to compare the injury risks predicted by the model to the proportion of injury cases observed in each test series.

Finally, once the injury prediction methods were tuned for the THUMS v4.1 and checked against the sled cases, we sought to apply the injury prediction method in an exemplar in-vehicle environment to demonstrate its use and observe the general magnitude of risk predicted. For this, we performed a simulation with the THUMS v4.1 in a driver environment derived from the National Highway Traffic Safety Administration's (NHTSA's) publicly available model of the 2014 Honda Accord [30]. The THUMS was seated in the driver position, and restraint was provided by a 3-point seatbelt (with pretensioner and force-limiter), the driver airbag, and the knee bolster (Figure 1). Simulations were performed with a pulse derived from a full-vehicle simulation of a 56 km/h impact into a full-width rigid barrier. The resulting thoracic injury risk predicted in that simulation was then contextualised by comparing to rib fracture injury risk reported in a past field data study.

TABLE I
PMHS TEST SERIES SELECTED FOR SIMULATION

Type	PMHS Test Series	Loading Condition	# of PMHS	Total # of Tests	# of tests with 3+ rib fractures
Impactor	[1314]	Rigid hub	38	38	30
	[15]	Rigid hub	3	3	3
	[16]	Rigid hub	7	7	5
	[17]	Rigid rod	3	3	3
	[18]	Rigid steering wheel rim	4	4	2
Table-Top	[19]	Rigid hub	15	18	3
		Distributed belt		16	1
		Single diagonal belt		18	2
		Double diagonal belt		15	2
	[20]	Load limited double diagonal belt	3	23	2
	[21]	Single diagonal belt	3	6	0
	[23-24]	Single diagonal belt	17	17	14
	[22]	Single diagonal belt	2	2	2
Sled	[25]	ΔV = 40 kph, 3-point standard belt	8	8	7
	[26]	ΔV = 30 kph, 3-point 3kN LL belt	5	5	2
		ΔV = 30 kph, 3-point 3kN LL belt Oblique frontal loading direction	3	3	2
	[29]	ΔV = 29 kph, 3-point standard belt	3	3	0
	[27]	ΔV = 48 kph, 3-point 3kN LL belt	3	3	3
	[28]	ΔV = 48 kph, 3-point standard belt	3	3	3

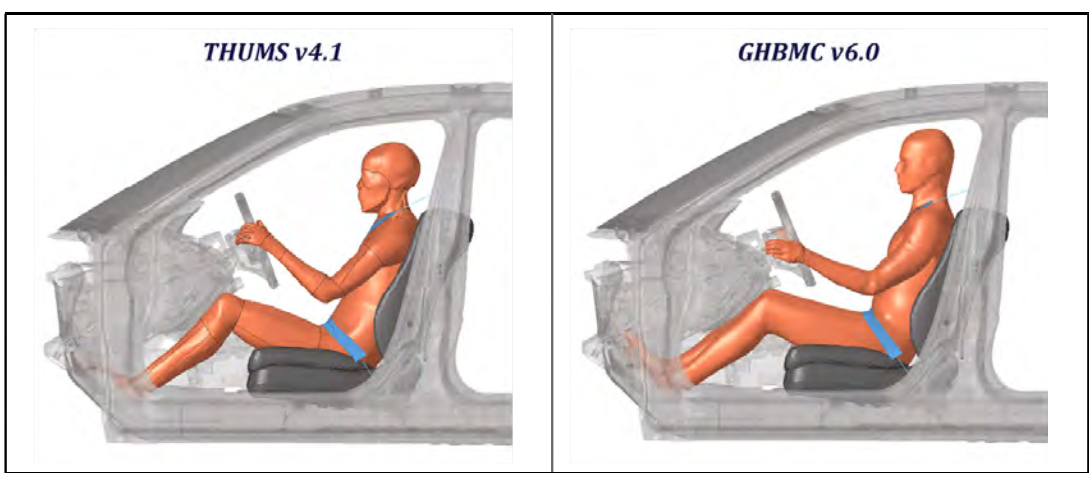

Fig. 1. THUMS v4.1 (left) and GHBMC v.6.0 (right) positioned in a vehicle occupant compartment model derived from NHTSA's publicly available model of the 2014 Honda Accord. Restraints included a pre-tensioned, force-limited 3-point belt, instrument panel, and driver airbag. Simulations were performed representing a 56 km/h full-width rigid barrier condition.

Injury Prediction Tuning & Evaluation

For this study, we sought to tune local strain-based injury prediction methods for application to the THUMS v4.1 and GHBMC v.6.0. For both models, the strains used were the 95th percentile maximum principal strains in each rib, with strain output from the middle integration point from the cortical bone shell elements. Compressive and tensile strains were considered together by taking the maximum of the absolute values of the maximum and minimum principal strains in each element. From that, the 95th percentile maximum principal strain was then calculated for each rib. The 95th percentile was chosen because it exhibits an attractive balance of having a strong likelihood of filtering out artificially high strains in particular elements (e.g., due to element quality issues or points of artificial stress concentration) while still being very straightforward to describe and apply consistently across models [31].

Following extraction of the strains, injury risk prediction was then based on the probabilistic approach developed by [8] and updated by [11]. This approach is comprised of the following basic steps (outlined in Figure 2):

1. Output the 95th percentile maximum principal strain in the cortical bone of each rib.
2. Using a local strain-based injury risk function, calculate the probability of fracture in each rib.
3. Combine the individual rib fracture probabilities to predict the probability of a select number of rib fractures, using a Poisson Binomial Model (also known as a Generalized Binomial Model).

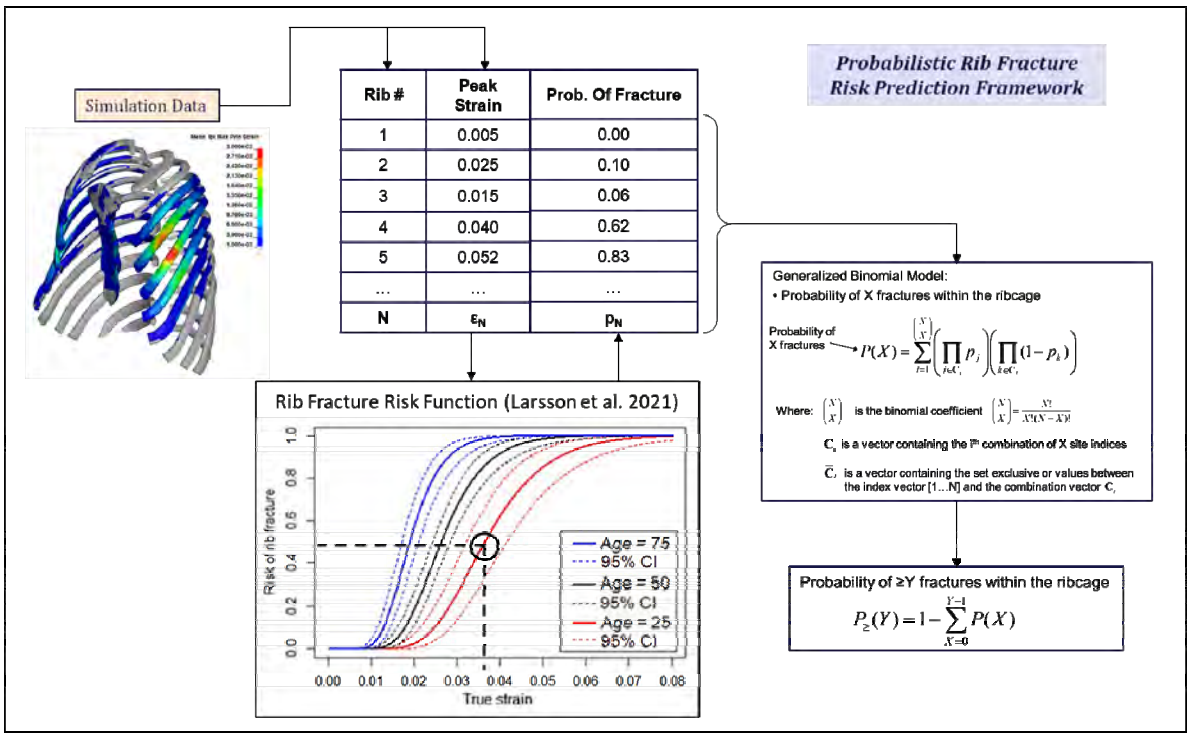

Fig. 2. Flowchart of probabilistic method to predict rib fracture risk using strain, combining local fracture probabilities from individual ribs to predict the risk of a selected number of fractures throughout the ribcage. This method was first developed by [8], and has since been updated with new data on rib cortical bone ultimate strain [11].

The original method developed by [8] used a local strain IRF based on a limited dataset of rib cortical bone coupon tests described by [32]. In 2021, reference [11] updated that local strain IRF using an expanded dataset of rib coupon tests, describing the ultimate strain distribution in a failure function using a Weibull distribution (with age as a covariate). The form of this function is shown in Equation 1. This served as the starting point for tuning the local strain IRF to arrive at the best fitting rib fracture prediction with the THUMS v4.1.

$$Weibull\ risk\,(strain, AGE) = 1 - exp\left(-\left(\frac{strain}{exp(\beta_0 + \beta_1 \cdot AGE)}\right)^{\alpha}\right) \quad (1)$$

The local strain IRF was then optimised to arrive at the best predictive fit between the 170 test-specific simulations, and the injuries observed in the matched PMHS tests. With a goal of making as few changes as were needed to arrive at reasonable model fit, the *shape* term (α) in Equation 1 was held constant (based on the value reported by [10]), and the β coefficients were modified via optimization to achieve the best injury prediction fit. During this process the PMHS age from each test was used in the calculation of risk from its matched simulation. The injury prediction fit was quantified using the log-likelihood summed across the 170 simulation-test pairs, with the sign flipped so that a smaller value would indicate a better model fit (termed here the summed negative log-likelihood, or SNLL). To accommodate the computational burden required to apply the probabilistic combined risk calculation to each datapoint for each iteration, the optimisation was performed using the surrogate optimisation function available in Matlab 2021 (function "surrogateopt"). The SNLL was used as the objective function, with a goal of minimizing the SNLL. The initial seed values for the optimization were the Weibull model coefficients reported by [10].

Two different severities of injury outcome were studied. The first was the predicted risk of threeor more fractured ribs. This was inspired by the current AIS definitions, where beginning in AIS version 2005 [7] three or more rib fractures were classified as an AIS severity level of 3 or greater. In addition, we considered the predicted risk of seven or more fractured ribs. This was inspired by the work of [33], who developed a thoracic IRF for application to the Hybrid III dummy based on the incidence of seven or more rib fractures observed in PMHS. While also based on a target of AIS3+ rib fracture injury, that study based their target severity outcome on earlier versions of the AIS dictionary that contained a different definition of how many rib fractures were needed to constitute a severity level of AIS 3 or greater [34]. That study also referenced earlier work that suggested that it may be expected that more rib fractures may be observed in PMHSs compared to living humans, either due to differences in diagnostic sensitivity or due to post-mortem changes in overall chest fragility, (i.w., from a loss of muscle tone. Combining the legacy AIS definition and the proposed PMHS-to-live occupant translation, [33] recommended that seven or more rib fractures observed in a PMHS be used as a surrogate outcome comparable to AIS 3+ rib fracture injury in a living human.

Predicting these two injury severity levels was approached in two ways. First, one of the unique benefits of the probabilistic strain-based approach of [8] is that it can be used to predict the risk of various severities of rib fracture injury based on a single underlying strain IRF. With this in mind, we first optimiseoptimised the local strain IRF based on concurrently fitting against the PMHS data at both the 3+ and 7+ rib fracture levels, i.e., seeking to arrive at a single strain-based IRF that provides the best balance of fit when predicting risk of 3+ fractures and when predicting risk of 7+ fractures. However, there is a possibility that there may be other factors that may confound prediction of multiple rib fracture severity levels from a single underlying strain IRF. To investigate this, we also performed additional optimisations to fit the local strain IRF targetting severity levels of 3+ fractures and 7+ fractures separately, i.e., one strain IRF tuned for prediction of 3+ fractures, and a different strain IRF tuned for prediction of 7+ fractures. These two methods (combined optimisation vs. separate optimisation) were then compared to observe if they would arrive a similar or different strain-based IRFs.

Aside from testing the fit against the 170 impactor and table-top tests that were used in the IRF development, prediction was qualitatively evaluated against two independent datasets. First, predictions were compared to PMHS injuries in simulations of the six sled test cases described above. This comprised a relatively small sample size – with a median of three PMHS tests per sled case, the percentage of cases exhibiting injury will be highly sensitive to outcomes in a single test, i.e., flipping from 0% injury to 33% injury based on a single PMHS. Thus, it is very difficult to draw meaningful quantitative inferences on the fit of an IRF against such data. It is possible, though, to qualitatively observe the general reasonableness of prediction against such data by examining the range of severities predicted, with relative ranking compared against the PMHS tests. One way to do this is with a reliability diagram, which plots the average risk predicted for a particular loadcase against the proportion of PMHSs in that loadcase that were observed to have injury (Figure 3). With reliability diagrams one may quickly observe if the predicted injury risk ranking is generally representative of the injuries observed, i.e., are cases of high predicted risk generally consistent with cases that resulted in a high number of injuries, and allows one to observe if the predicted risk is generally biased towards underprediction or overprediction, or tends to fall evenly between the two. In addition, the general magnitude of injury prediction in the 56 km/h vehicle occupant compartment simulation was compared against risks predicted from a recent field data study. These comparisons to the sled cases and the field data served to place in context the general reasonableness of the

risks predicted from these IRFs, indicating whether or not they are consistent with the general magnitude of risk that should be expected in such cases.

Finally, the ultimate goal of this work was to develop an IRF-tuning pipeline that can be applied to any human body model. To assess the usability of this pipeline with another human body model, the process described above was repeated with the GHBMC v6.0 model. The 170 component load cases were simulated with the GHBMC v.6.0, and a local strain IRF was optimiseoptimised for the GHBMC in the same manner as described above. The GHBMC model was also subjected to the in-vehicle simulation shown in Figure 1, and the resulting injury risks predicted with the GHBMC were compared to those predicted with THUMS (each using their own tuned strain IRFs).

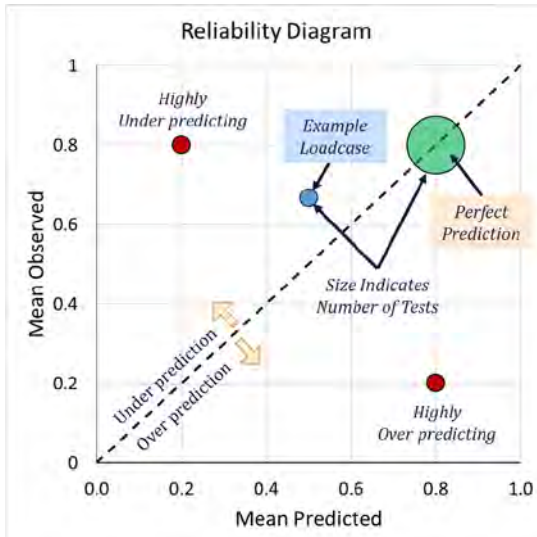

Fig. 3. Reliability diagram, used to qualitatively observe the nature of over-prediction or under-prediction of a model compared to groups of observations. In our case, each datapoint represents a particular load case, containing a collection of PMHS tests within that loadcase. The *Mean Predicted* is the average risk of the outcome of interest (either 3+ fractures or 7+ fractures) predicted by the model for that loadcase. The *Mean Observed* is the percentage of PMHSs within that loadcase that exhibited the outcome of interest. (For example, if 6 out of 10 PMHSs within a particular loadcase exhibited three or more fractures, then the *Mean Observed 3+ Fx*. for that load case would be 6/10=0.6.)

III. RESULTS

The one hundred and seventy test-specific impactor and table-top simulations were performed successfully. As described above, the 95th percentile maximum and minimum principal strains were then extracted from each of the ribs, and the local strain IRF was then optimised to provide the best fit to the occurrence of 3+ and 7+ rib fractures observed in the matched experiments (with translation between the local strain IRF and predicted risk of a collection of rib fractures occurring via the combined probability method of [8]). The results of that optimisation are shown in Figure 4, compared to the original strain-based IRF that [11] derived from rib cortical bone coupon tests. As can be seen in Figure 4, the optimisation indicated that the local strain IRF should be shifted substantially to the left compared to the original curve [11] to result in the best prediction fit with THUMS v4.1.

Figure 4 also shows a comparison of the two different methods of optimisation discussed above – optimising in a combined approach seeking to predict the risk of 3+ and 7+ fractures with one local strain function, and optimising the local strain function for 3+ fractures and 7+ fractures separately. As can be seen in Figure 4, there was a noticeable difference between the two approaches. With the separate optimisation, the local strain curve for prediction of 7+ fractures is to the left of the curve for prediction of 3+ fractures. The local strain IRF derived from combined, concurrent optimisation is in between the two independently optimiseoptimised functions.

The separate optimisation resulted in better fit as indicated by the summed log-likelihood. The coefficients for the individually-optimised curves are shown in Table II (note: to avoid potential confusion that may result from presenting multiple candidate IRFs, we are choosing to only present the coefficients from the best fitting

models).

The six sled simulations were also performed successfully. As shown in Appendix A, the THUMS v4.1 exhibited reasonable biofidelity in its interaction with the simulated test environments (as indicated by examining the belt forces and kinematics compared to the PMHS tests). The rib strains were output and the rib fracture risk was calculated using the optimised functions described above. The reliability diagrams of Figure 5 show the results of this prediction, compared to the proportion of test subjects that exhibited the target injury levels.

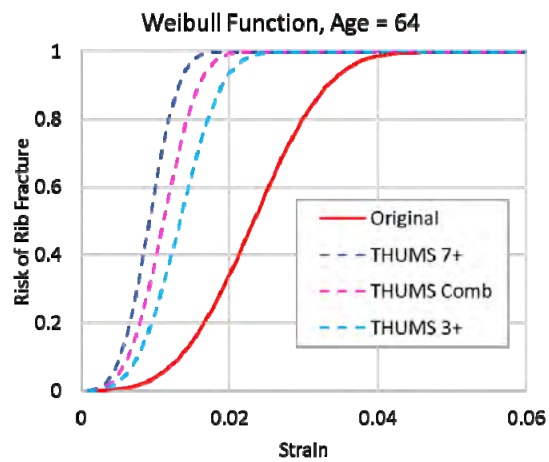

Fig. 4. Local strain-based fracture risk functions, comparing the original local failure curve described by [11] (derived from rib material property tests; solid red line) to a set of local failure curvesoptimised for prediction with the THUMS v4.1 (dashed lines). The three THUMS curves show various means of optimising the local failure curves, including taking a combined approach seeking to optimise one function to predict both 3+ and 7+ fractures, versus developing separate curves each optimised to either provide the best fit for 3+ fracture prediction or 7+ fracture prediction. The functions are plotted for the average age of the PMHS tests (age 64).

TABLE II

FINALISED PARAMETERS FOR THE WEIBULL FRACTURE RISK FUNCTIONS TO BE USED IN THE STRAIN-BASED PROBABILISTIC RIB FRACTURE PREDICTION FRAMEWORK WITH THE THUMS V4.1 MODEL

	β0	β1	α
3+ Rib fractures injury level	-3.0665	-0.0179	3.3562
7+ Rib fractures injury level	-3.72	-0.0135	3.3562

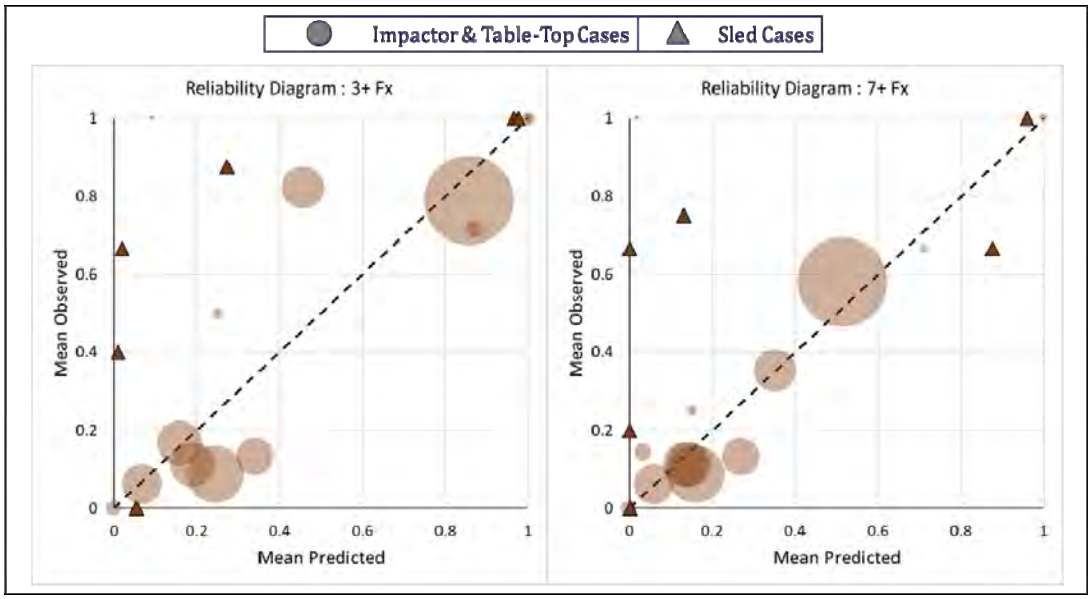

Fig. 5. Reliability diagrams comparing the predicted risks to the proportion of tests with the outcomes of interest. The circles are loadcases that were used in the tuning of the local strain-based failure functions (the impactor and table-top cases; the diameter indicates the number of tests in each loadcase). The triangles are sled loadcases that were not used in the model tuning.

On applying this simulation and analysis pipeline to the GHBMC v.6.0, the strain-IRF optimised for the GHBMC ended up closer to the rib cortical bone ultimate strain function described by [11]. The coefficients for the combined strain IRF model tuned for the GHBMC are shown in Table III. Figure 5 shows this function compared to the ultimate strain distribution of Larsson et al. [11], as well as the combined local strain IRF tuned for THUMS v.4.1.

TABLE III
LOCAL STRAIN IRF PARAMETERS TUNED FOR THE GHBMC V.6.0

	β0	β1	α
Combined optimisation for 3+ and 7+ fractures	-3.27987	-0.00663	3.3562

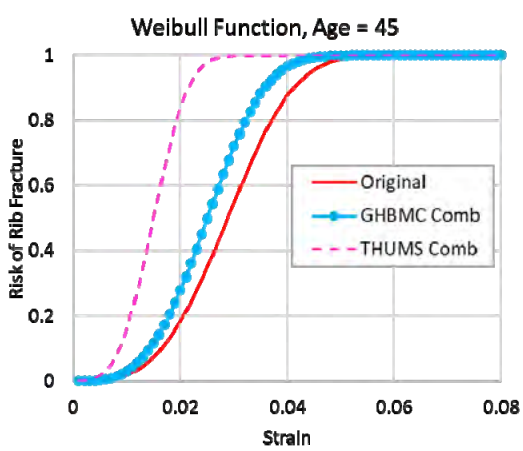

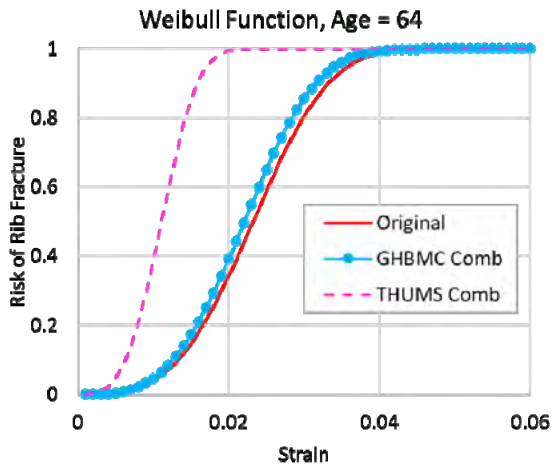

Fig. 6 Local strain-based fracture risk functions, comparing the original local failure curve described by [11] (derived from rib material property tests; solid red line) to a set of local failure curves optimised for prediction with the THUMS v4.1 (dashed red line), and the GHBMC v.6.0 (blue line with circle markers). For comparison purposes, both of the THUMS and GHBMC curves shown here are those developed using a combined optimisation for prediction of 3+ and 7+ rib fractures. The functions are plotted for the average age of the PMHS tests (age 64).

Finally, a 56 km/h frontal impact simulation was performed with the THUMS v4.1 and the GHBMC v.6.0 placed in the driver seat of a sled-type model developed from NHTSA's 2014 Honda Accord FE model (belted, with a driver airbag). The 95th percentile maximum principal strains observed in each rib of each model are shown in Appendix D. Table IV and Table V show the rib fracture risks calculated from the rib strains resulting from those simulations. For comparison, the risk of AIS 3+ rib fracture derived from field data was also calculated, based on the multi-variate regression models developed by [4]. That field data model was developed from an analysis of frontal impact collisions with belted occupants from NASS-CDS 1998-2015. The risk estimates below were calculated assuming a mid-sized male occupant in a vehicle of model year 2009 or newer, in a collision with a 56 km/h ΔV (Table IV and V).

TABLE V

RIB FRACTURE RISKS PREDICTED BY THUMS V.4.1 IN A 56 KM/H FRONTAL COLLISION WITH A MODERN SEATBELT AND AIRBAG (COMPARED TO INJURY RISK IN A SIMILAR COLLISION BASED ON FIELD DATA [4]*)

Age	THUMS v4.1		Field Data [4]
	Risk of 3+ Rib Fx	*Risk of 7+ Rib Fx*	*Risk of AIS3+ Rib Fx.**
25 y/o	0.1 %	<0.01%	0.3%
45 y/o	2.4 %	0.1 %	1.4%
65 y/o	27.9 %	5.0 %	6.2%

* Risk calculated for a mid-sized, belted male in a vehicle of model year 2009 or newer

TABLE V

RIB FRACTURE RISKS PREDICTED BY GHBMC V.6.0 IN A 56 KM/H FRONTAL COLLISION WITH A MODERN SEATBELT AND AIRBAG (COMPARED TO INJURY RISK IN A SIMILAR COLLISION BASED ON FIELD DATA [4]*)

Age	GHBMC v.6.0		Field Data [4]
	Risk of 3+ Rib Fx	Risk of 7+ Rib Fx	Risk of AIS3+ Rib Fx.*
25 y/o	0.8 %	<0.01%	0.3%
45 y/o	2.7 %	<0.01 %	1.4%
65 y/o	7.8 %	<0.01 %	6.2%

* Risk calculated for a mid-sized, belted male in a vehicle of model year 2009 or newer

IV. DISCUSSION

To be useful tools for injury assessment, any occupant model (be it physical or computational) requires means

to interpret its measurements to predict injury risk. The relationship between a model's resulting internal measures and the external applied loading are dependent on the specific construction and mechanical properties of the model. As a result, it is also likely that the relationship between a model's internal measures and predicted injury risk (for a real person in a matched collision) would also be dependent on the specific construction of the model. Just as similar chest deflections from different ATD designs may not represent similar risks of injury, we should expect that different computational model designs may require different injury risk functions to arrive at comparable injury prediction.

For dummies, tuning of injury risk functions is often accomplished by performing matched dummy tests and PMHS tests, and optimising a function to relate the dummy internal measures to injuries observed in the PMHS [35-36]. We take a similar approach in the framework that we have developed here, performing a large number of simulations targetting matched PMHS tests and optimising strain-based IRFs to best fit the observed injuries. The result of this tuning was that the local strain IRFs tuned for THUMS v4.1 were substantially to the left of the local rib cortical bone ultimate strain distribution reported by [11]. This means that, when compared to the actual strain tolerance of rib cortical bone, the THUMS v4.1 needs less rib strain to arrive at an appropriate prediction of injury risk observed in matched PMHS tests. If one were to apply the [11] ultimate strain function to THUMS v4.1 directly, that would result in a substantial underestimation of rib fracture risk in the PMHS dataset used here. In contrast, the local strain IRF tuned for GHBMC v.6.0 was much closer to the ultimate strain curve of [11], meaning that more strain is required in the GHBMC (compared to THUMS) to result in a comparable predicted risk of injury. Thus, while the cortical bone ultimate strain distribution of [11] may serve as a reasonable starting point for investigation, these results suggest that such a function's predictive ability should be critically evaluated when applied to a new model, and if necessary should be tuned based on the rib strains experienced in that model.

Note that this is not necessarily indicative of a limitation in biofidelity of either model, as biofidelity can mean many different things. For example, the THUMS v4.1 has been shown to be biofidelic in the force-compression response of its chest under multiple impactor and belt loading modes. However, strain-based injury prediction is also dependent on the relationship between gross ribcage deflection and strain induced in models of the ribs. This is partially dependent on the fundamental mechanics of the rib models, but is also partially dependent on model-specific factors that may affect rib strain (such as the mesh density). By taking the IRF-tuning approach developed here, a model does not necessarily need to replicate rib strains that an actual vehicle occupant would experience. It is sufficient instead for the model to be biofidelic in its gross response (to ensure that it interacts with its environment in a biofidelic way) and for the relative magnitude of strain in its ribs to be sensitive to the severity and pattern of loading in a manner consistent with PMHSs. This potentially provides a means to tune injury prediction across models of differing complexity, without needing to validate each down to the rib-strain level.

While the combined probability method of [8] (Figure 2) allows the possibility to predict the risk of different numbers of rib fractures using a single local strain IRF, the results presented here suggest that better-fitting prediction may be accomplished by fitting separate local strain IRFs for prediction of 3+ fractures and 7+ fractures. This is to be expected, since by fitting separate functions, we are essentially doubling the number of degrees of freedom, i.e., function coefficients, in the prediction model, which by definition will always result in a better fit (when evaluated against the data that is used in the model fitting). The fact that the THUMS local strain functions tuned for 3+ fractures and 7+ fractures are different means that the relationship between strain observed in the model and the predicted severity of injury is nonlinear. The local strain IRF tuned for prediction of 7+ fractures is to the left of the local strain function tuned for the prediction of 3+ fractures. This means that less incremental increase in strain per rib is needed to escalate from 3 fractures to 7 fractures, compared to the strain needed to escalate from 0 fractures to 3 fractures. This may be a function of loss of stability in the ribcage that may occur with large numbers of rib fractures. In PMHSs, as ribs begin to break the internal load is transferred to the surrounding ribs, eventually compromising the overall structural stability of the chest. This phenomenon is not replicated in these simulations, as the probabilistic rib fracture prediction approach is implemented without a singular definition of fracture in the ribs. As the structural stability of the ribcage is increasingly compromised in PMHSs, a modest increase in overall loading severity may result in continuing accumulation of more fractures. In the human body models (which maintain ribcage stability throughout the simulations), this translates to needing lesser incremental increase in per-rib strain to continue to accumulate

predicted risk of more rib fractures. This phenomenon is just a hypothesis at this point, and may be checked in future work implementing a combined approach where element elimination is utilised in ribs that exhibit a very high predicted risk of fracture. Other statistical methods may also be examined to combine rib fracture probabilities accounting for potential dependence in individual fracture outcomes.

The first bar to pass when evaluating the potential utility of an injury prediction tool is demonstrating that it has a reasonable ability to discriminate events that have a very high risk of injury, compared to events that have a very low risk of injury. The reliability diagrams of Figure 5 suggest that the independently-tuned local strain IRFs, applied to THUMS v4.1 pass this bar. When applied to the sled cases that resulted in injury in all of the PMHSs tested (defined by either 3+ or 7+ fractures), the strain-based method predicted nearly 100% risk of injury. Similarly, when applied to the sled case that did not result in injuries to any of the PMHSs tested, the simulations predicted nearly 0% risk of injury. The greatest differences were observed in the transition region, in three sled cases (all of the *Gold-Standard* style; [25-26]) that resulted in injuries to some of the PMHSs despite a very low risk predicted by the models. This is likely reflective of the challenge of evaluating predictive ability of a model using a small number of PMHS tests. In any one of the three sled cases where differences were observed, flipping one or two tests from injury to non-injury may result in a substantial change in the perceived predictive ability of the model. Thus, the comparison may be at the mercy of the specific characteristics and fragility of a small number of PMHSs. This is in contrast to the dataset used for the model fitting, which by its size (170 tests) will be much less sensitive to any single outcome. Future work may warrant continuing expansion of the evaluation dataset as new PMHS tests become available (in these and other loading modes), to provide a basis for evaluation of strain IRFs tuned for THUMS and other HBMs that moves closer towards a population-level assessment. Additional data collection should focus on the transition region for injury risk (both for model fitting and evaluation), to improve the fidelity of discriminating finer differences in risk.

The ultimate test of an injury prediction tool lies in proving its ability to predict injury risk in the field. While that is a complex and daunting task (well beyond the scope of this particular study), the exemplar 56 km/h simulations in the 2014 Accord vehicle environment suggests that the rib fracture risks predicted with the tuned strain IRFs are at least generally consistent with the rib fracture risk estimated for similar conditions in the field. As noted above, there have been various means proposed to link AIS3+ rib fracture severity conditions to data from PMHS tests [33-36]. These definitions of AIS3+ injury have ranged from ≥3 rib fractures [36] to ≥7 rib fractures [33] observed in PMHS tests. As shown in Table IV, the AIS3+ rib fracture risks estimated from the field data tended to fall near or between the 3+ and 7+ rib fracture risks predicted with both the THUMS v.4.1 and GHBMC v.6.0. In addition, the strain IRFs tuned for both models tended to exhibit a sensitivity to age similar to that observed in the field data. While there are many factors that likely confound the direct comparison between model results and field data, the similarity in both magnitude and age-effect gives confidence that the model-derived risk estimates are at least reasonable. Future efforts may warrant extending this analysis to compare to field-derived risks in a manner that includes variability in collision and occupant characteristics using large-scale parametric simulation [10][37].

The ultimate goal of this study was to develop a pipeline to tune local strain IRFs for application to specific human body models, seeking to arrive at comparable levels of injury risk prediction despite differences in model construction. Though some differences remain, the results of the in-vehicle simulations indicate that this study has made substantial progress towards that goal. In matched simulations, the GHBMC v.6.0 tends to systematically result in greater rib maximum principal strains than the THUMS v.4.1. This is reflected in the local strain IRFs developed from the impactor and table-top simulations, where a particular level of rib fracture risk is correlated to greater strains in the GHBMC compared to the THUMS. This is also reflected in the results of the in-vehicle simulations, where the GHBMC exhibited greater maximum principal strains in most of the ribs (Appendix D). However, by using local strain IRFs tuned for each IRF, the GHBMC and THUMS both resulted in predicted injury risk comparable to the field data observations, despite the substantial differences in strain observed in each model. The risks predicted with the THUMS v.4.1 were on the high end of the field data observations, and the risks predicted with the GHBMC v.6.0 were on the low end of the field data observations, but both were consistent with the field data within the range of uncertainty associated with rib fracture definitions described above. Considering that this analysis was performed with two different models, exhibiting different rib strains, each with unique local strain IRFs based on their specific characteristics – that either would be remotely consistent with field data is itself a substantial feat. That both are consistent with field data (within

a logical range of uncertainty) suggests that this method has been successful in advancing a means to arrive at comparable injury prediction across two HBMs, despite substantial differences in construction and response. We encourage others to continue to look for ways to refine this methodology, driving towards comparable injury prediction across a diversity of models.

Finally, this study focused on loading modes that resulted in predominantly frontal loading to the chest. As such, until their predictive ability can be evaluated in other loading modes, the local strain IRFs developed here should be confined to applications of frontal impact loading, similar to the cases within the dataset of this study. One of the potential benefits of strain-based injury prediction methods, however, is that it is possible that they may be used for injury prediction across a diversity of loading modes, including different loading directions. While the dataset used in this study was confined to frontal impacts, the overall framework is certainly not. With the framework developed here, the dataset may be expanded to include PMHS tests under other loading conditions, including different directions and patterns of loading. This framework may also be applied to tune strain-based IRFs for other body regions, particularly those that may benefit from a combined probability approach due to complex structures, strain fields, and the potential for different types of fracture that may occur (for example, tuning local strain IRFs for a combined probability approach in the pelvis).

V. CONCLUSIONS

This study developed a framework to tune local strain IRFs for specific human body models, seeking to arrive at comparable thoracic injury risk prediction across HBMs of differing construction. This study performed 170 simulations across 13 impactor and table-top load cases to serve as a basis to tune the local strain IRFs (demonstrated first with the THUMS v4.1, and then also applied to the GHBMC v.6.0), and examined the general predictive ability of the resulting IRFs in selected whole-body sled and vehicle simulations. The results suggested that direct application of rib cortical bone ultimate strain data to the THUMS v4.1 would result in underestimation of rib fracture risk compared to the reference PMHS tests. Tuning the local strain IRF for application to THUMS v4.1., however, tended to result in reasonable injury risk prediction compared to PMHS results and compared to risks derived from field data. Tuning the local strain IRF for the GHBMC v.6.0 resulted in a function closer to the ultimate strain of rib cortical bone, requiring more strain to arrive at comparable injury risk prediction compared to the THUMS. By tuning the local strain IRFs for each of these human body models, each model was able to arrive at injury risk prediction comparable to field data estimates when applied to a vehicle simulation environment. This is the first effort, to our knowledge, to develop a standardised framework to tune rib fracture IRFs to arrive at comparable injury risk prediction across human body models. Future efforts may include expanding this dataset to incorporate additional loading modes, and applying these methods with other HBMs.

VI. ACKNOWLEDGEMENT

This work was supported by the Toyota Collaborative Safety Research Center. (U.S.A.) All opinions here are solely those of the authors.

VII. REFERENCES

[1] Andriacchi, T., Schultz, A., Belytschko, T., and Galante, J. (1974). A model for studies of mechanical interactions between the human spine and rib cage. J. Biomech., 7(6), 497-507.

[2] Plank, G. R., and Eppinger, R. (1989). Computed dynamic response of the human thorax from a finite element model. 12th Proceedings, International Technical Conference on the Enhanced Safety of Vehicles, 665-672.

[3] Iwamoto, M., Kisanuki, Y., Watanabe, I., Furusu, K., Miki, K., & Hasegawa, J. (2002, September). Development of a finite element model of the total human model for safety (THUMS) and application to injury reconstruction. In *Proceedings of the international IRCOBI Conference* (pp. 18-20).

[4] Forman, J., Poplin, G. S., Shaw, C. G., McMurry, T. L., Schmidt, K., Ash, J., & Sunnevang, C. (2019). Automobile injury trends in the contemporary fleet: Belted occupants in frontal collisions. *Traffic Injury Prevention*, *20*(6), 607-612.

[5] Forman, J. L., & McMurry, T. L. (2018). Nonlinear models of injury risk and implications in intervention targeting for thoracic injury mitigation. *Traffic injury prevention*, *19*(sup2), S103-S108.

[6] Pipkorn, B., Iraeus, J., Lindkvist, M., Puthan, P., & Bunketorp, O. (2020). Occupant injuries in light passenger vehicles—A NASS study to enable priorities for development of injury prediction capabilities of human body models. *Accident Analysis & Prevention*, *138*, 105443.

[7] The Abbreviated Injury Scale, 2005. Association for the Advancement of Automotive Medicine. Barrington, IL.

[8] Forman, J. L., Kent, R. W., Mroz, K., Pipkorn, B., Bostrom, O., & Segui-Gomez, M. (2012, October). Predicting rib fracture risk with whole-body finite element models: development and preliminary evaluation of a probabilistic analytical framework. In Annals of Advances in Automotive Medicine/Annual Scientific Conference (Vol. 56, p. 109). Association for the Advancement of Automotive Medicine.

[9] Guleyupoglu, B., Koya, B., Barnard, R., & Gayzik, F. S. (2018). Failed rib region prediction in a human body model during crash events with precrash braking. *Traffic injury prevention*, *19*(sup1), S37-S43.

[10] Pipkorn, B., Iraeus, J., Björklund, M., Bunketorp, O., & Jakobsson, L. (2019). Multi-scale validation of a rib fracture prediction method for human body models. In *Proceedings of the IRCOBI Conference* (pp. 175-192).

[11] Larsson, K. J., Blennow, A., Iraeus, J., Pipkorn, B., & Lubbe, N. (2021). Rib cortical bone fracture risk as a function of age and rib strain: updated injury prediction using finite element human body models. Frontiers in bioengineering and biotechnology, 9, 412.

[12] Panzer, M. B., Myers, B. S., Capehart, B. P., & Bass, C. R. (2012). Development of a finite element model for blast brain injury and the effects of CSF cavitation. Annals of biomedical engineering, 40(7), 1530-1544.

[13] Kroell, C. (1971). Impact tolerance and response of the human thorax. In Proc. 15th Stapp Car Crash Conference, 1971 (pp. 84-134).

[14] Kroell, C. K., Schneider, D. C., & Nahum, A. M. (1974). Impact tolerance and response of the human thorax II. SAE Transactions, 3724-3762.

[15] Horsch, J. D., & Schneider, D. (1988). Biofidelity of the Hybrid III Thorax in high-velocity frontal impact. SAE transactions, 169-176.

[16] Yoganandan, N., Pintar, F. A., Kumaresan, S., Haffiner, M., & Kuppa, S. (1997). Impact biomechanics of the human thorax-abdomen complex. International journal of crashworthiness, 2(2), 219-228.

[17] Hardy, W. N., Schneider, L. W., & Rouhana, S. W. (2001). Abdominal impact response to rigid-bar, seatbelt, and airbag loading. Stapp car crash journal, 45, 1-32.

[18] Shaw, G., Lessley, D., Bolton, J., & Crandall, J. (2004). Assessment of the THOR and Hybrid III crash dummies: Steering wheel rim impacts to the upper abdomen (No. 2004-01-0310). SAE Technical Paper.

[19] Kent, R., Lessley, D., & Sherwood, C. (2004). Thoracic response to dynamic, non-impact loading from a hub, distributed belt, diagonal belt, and double diagonal belts. Stapp car crash journal, 48, 495.

[20] Forman, J., Kent, R., Ali, T., Crandall, J., Bostrom, O., & Haland, Y. (2005). Biomechanical considerations for the optimisation of an advanced restraint system: assessing the benefit of a second shoulder belt. In IRCOBI Conference on the Biomechanics of Impact.

[21] Salzar, R. S., Bass, C. R., Lessley, D., Crandall, J. R., Kent, R. W., & Bolton, J. R. (2009). Viscoelastic response of the thorax under dynamic belt loading. Traffic injury prevention, 10(3), 290-296.

[22] Kemper, A. R., Kennedy, E. A., McNally, C., Manoogian, S. J., Stitzel, J. D., & Duma, S. M. (2011). Reducing chest injuries in automobile collisions: rib fracture timing and implications for thoracic injury criteria. Annals of biomedical engineering, 39(8), 2141-2151.

[23] Cesari, D., & Bouquet, R. (1990). Behaviour of human surrogates thorax under belt loading (No. 902310). SAE Technical Paper.

[24] Cesari, D., & Bouquet, R. (1994). Comparison of Hybrid III and human cadaver thorax deformations loaded by a thoracic belt. SAE transactions, 1633-1644.

[25] Shaw, G., Parent, D., Purtsezov, S., Lessley, D., Crandall, J., Kent, R., ... & Martin, P. (2009). Impact response of restrained PMHS in frontal sled tests: skeletal deformation patterns under seat belt loading. Stapp Car Crash Journal, 53, 1.

[26] Acosta, S. M., Ash, J. H., Lessley, D. J., Shaw, C. G., Heltzel, S. B., & Crandall, J. R. (2016). Comparison of whole body response in oblique and full frontal sled tests. In Proceedings of IRCOBI Conference.

[27] Forman, J., Lopez-Valdes, F., Lessley, D., Kindig, M., Kent, R., Ridella, S., & Bostrom, O. (2009). Rear seat occupant safety: an investigation of a progressive force-limiting, pretensioning 3-point belt system using adult PMHS in frontal sled tests. Stapp car crash journal, 53, 49.

[28] Michaelson, J., Forman, J., Kent, R., & Kuppa, S. (2008). Rear seat occupant safety: kinematics and injury of PMHS restrained by a standard 3-point belt in frontal crashes (No. 2008-22-0012). SAE Technical Paper.

[29] Forman, J., Lessley, D., Shaw, C. G., Evans, J., Kent, R., Rouhana, S. W., & Prasad, P. (2006). Thoracic response of belted PMHS, the Hybrid III, and the THOR-NT mid-sized male surrogates in low-speed, frontal crashes (No. 2006-22-0009). SAE Technical Paper.

[30] Singh, H., Ganesan, V., Davies, J., Paramasuwom, M., & Gradischnig. (2018, May). Vehicle interior and restraints modeling development of full vehicle finite element model including vehicle interior and occupant restraints systems for occupant safety analysis using THOR dummies (Report No. DOT HS 812 545). Washington, DC: National Highway Traffic Safety Administration https://www.nhtsa.gov/crash-simulation-vehicle-models

[31] Iraeus, J., & Pipkorn, B. (2019). Development and validation of a generic finite element ribcage to be used for strain-based fracture prediction. In Proceedings of the IRCOBI Conference (pp. 193-210).

[32] Kemper, A. R., McNally, C., Kennedy, E. A., & Manoogian, S. J. (2005). Material Properties of Human Rib Cortical Bone from Dynamic Tension Coupon Testing. Stapp Car Crash Journal, 49, 199.

[33] Laituri, T. R., Prasad, P., Sullivan, K., Frankstein, M., & Thomas, R. S. (2005). Derivation and evaluation of a provisional, age-dependent, AIS3+ thoracic risk curve for belted adults in frontal impacts. SAE Technical Paper, (2005-01), 0297.

[34] The Abbreviated Injury Scale, 1990 Revision, Update 1998. Association for the Advancement of Automotive Medicine. Des Plaines, IL.

[35] Kent, R., Patrie, J., & Benson, N. (2003). The Hybrid III dummy as a discriminator of injurious and non-injurious restraint loading. In Annual Proceedings/Association for the Advancement of Automotive Medicine (Vol. 47, p. 51). Association for the Advancement of Automotive Medicine.

[36] Poplin, G. S., McMurry, T. L., Forman, J. L., Ash, J., Parent, D. P., Craig, M. J., ... & Crandall, J. (2017). Development of thoracic injury risk functions for the THOR ATD. Accident Analysis & Prevention, 106, 122-130.

[37] Perez-Rapela, D., Forman, J. L., Huddleston, S. H., & Crandall, J. R. (2020). Methodology for vehicle safety development and assessment accounting for occupant response variability to human and non-human factors. Computer methods in biomechanics and biomedical engineering, 24(4), 384-399.

VIII. APPENDIX

Appendix A: Brief Illustrations of Loadcases Simulated in this Study

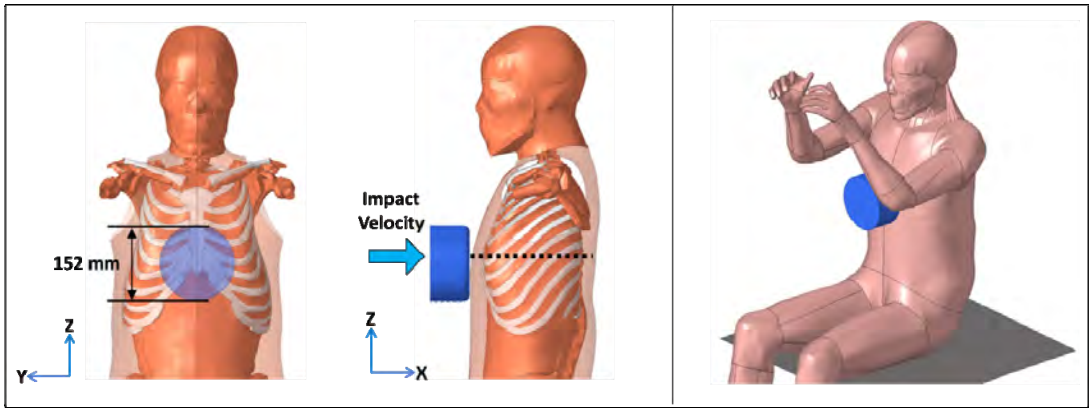

Fig. A1. Hub impactor case of [12-1415].

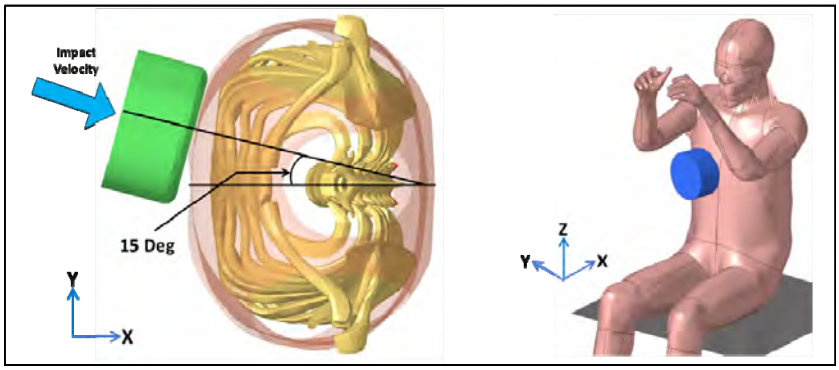

Fig. A2: Oblique hub impactor case of [16].

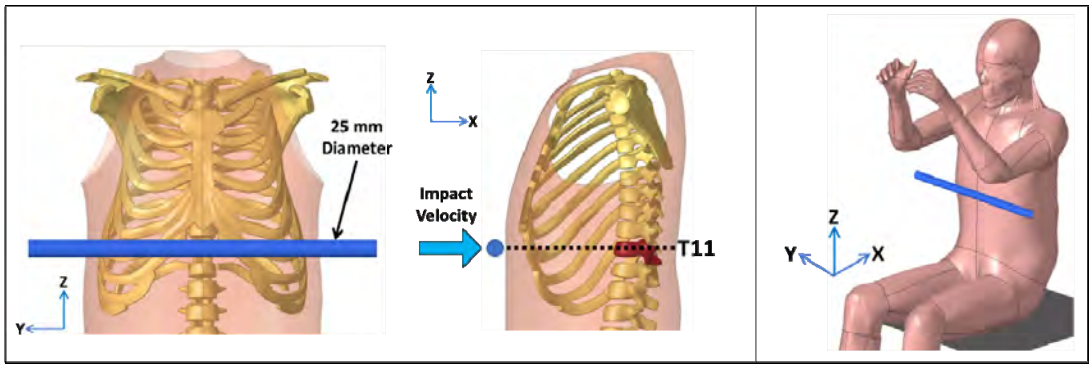

Fig. A3. Rigid rod impactor case of [17].

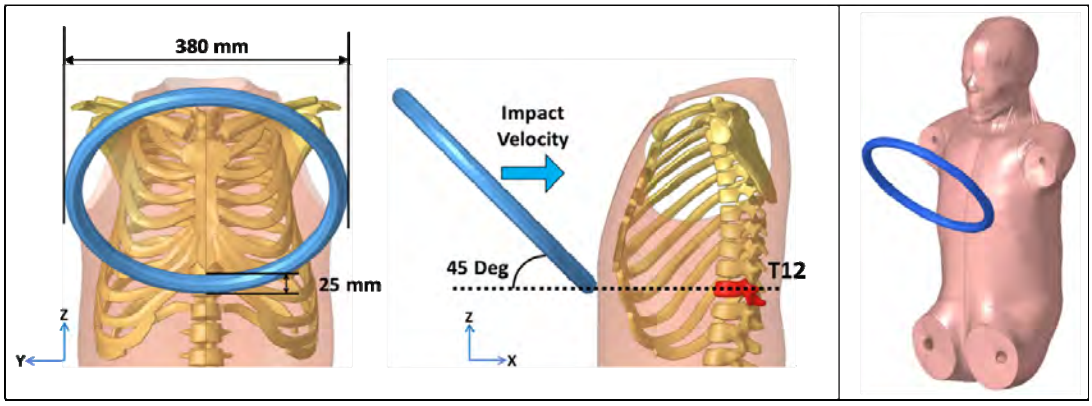

Fig. A4. Steering wheel rim impactor case of [18].

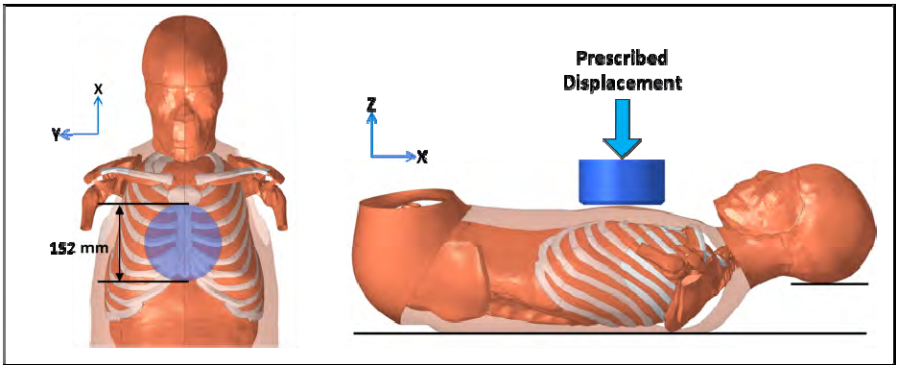

Fig. A5. Table-top hub loading case of [19].

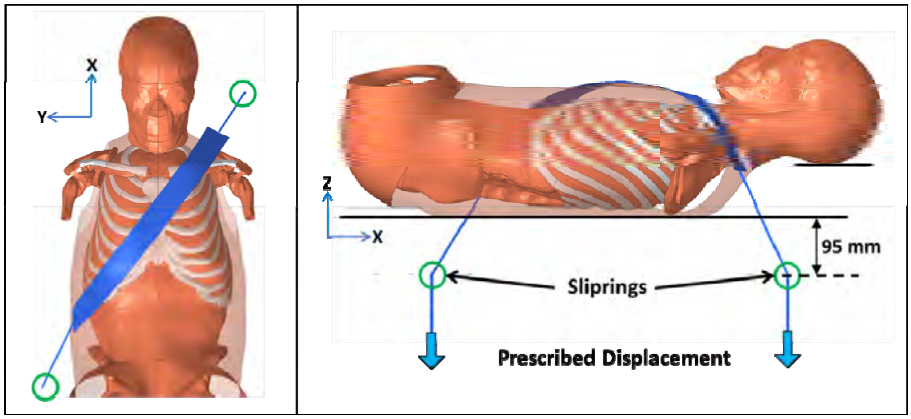

Fig. A6. Table-top single-diagonal-belt case of [19].

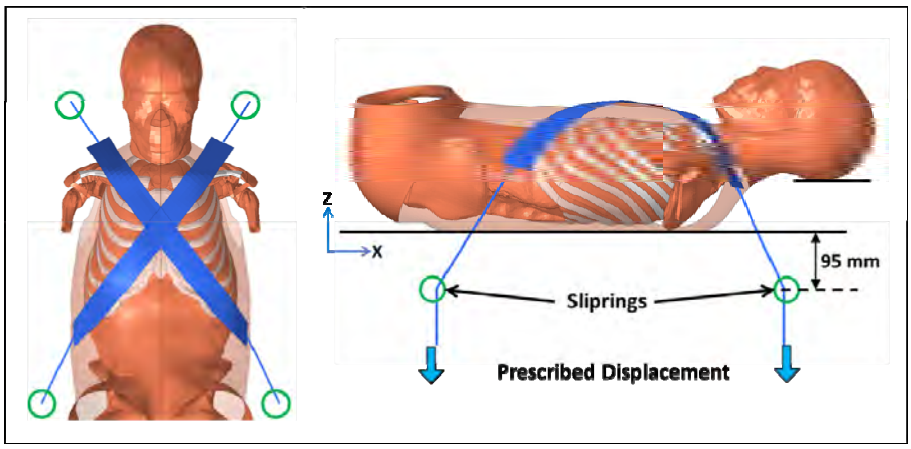

Fig. A7. Table-top double-diagonal-belt case of [19].

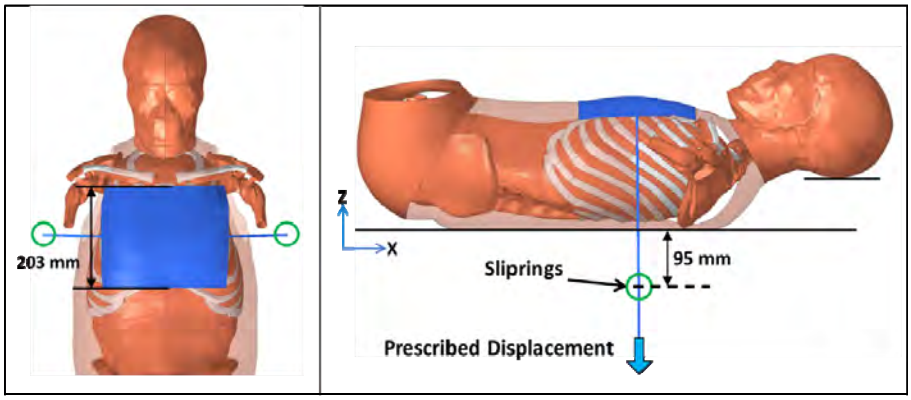

Fig. A8. Table-top distributed belt case of [19].

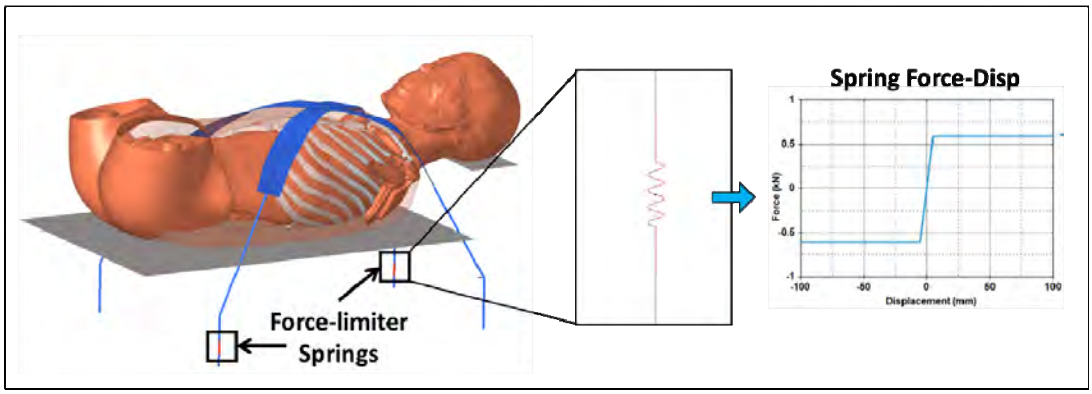

Fig. A9. Table-top double-diagonal-belt case of [20], with force-limiting in one of the belts (to result in differential force application).

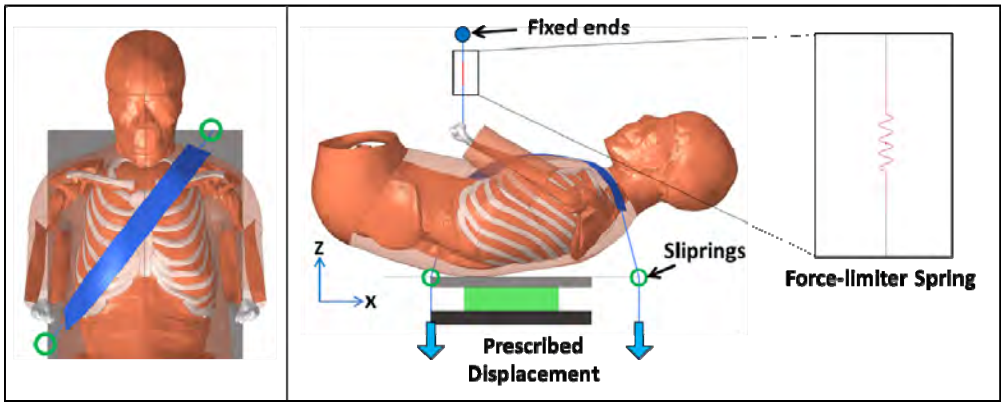

Fig. A10 Table-top single-diagonal-belt case of [21], with a rigidly-constrained spine and anteriorly-supported arms.

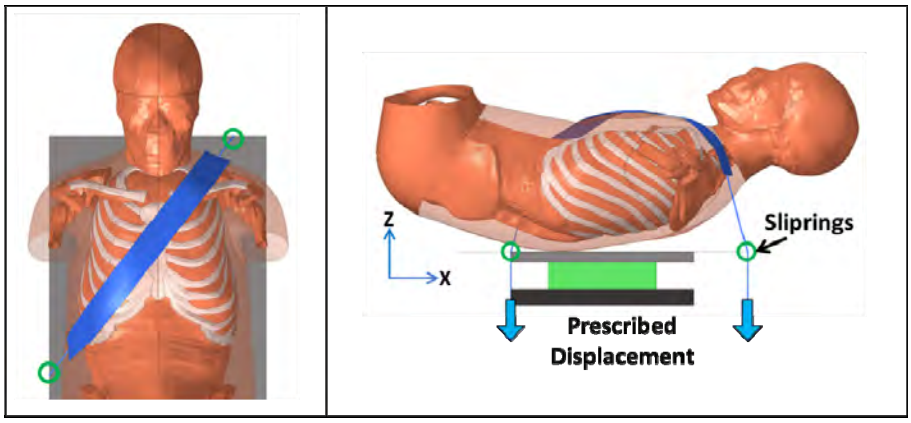

Fig. A11. Table-top single-diagonal-belt case of [22], with a rigidly-constrained spine.

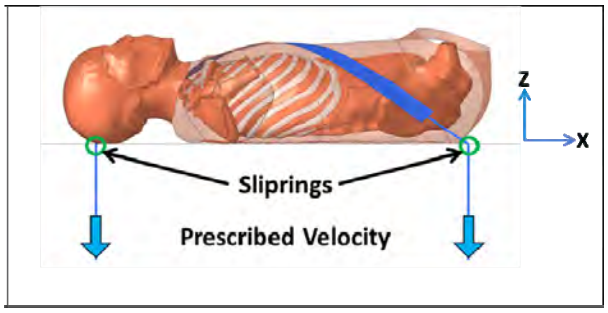

Fig. A12. Table-top single-diagonal-belt case of [23-24].

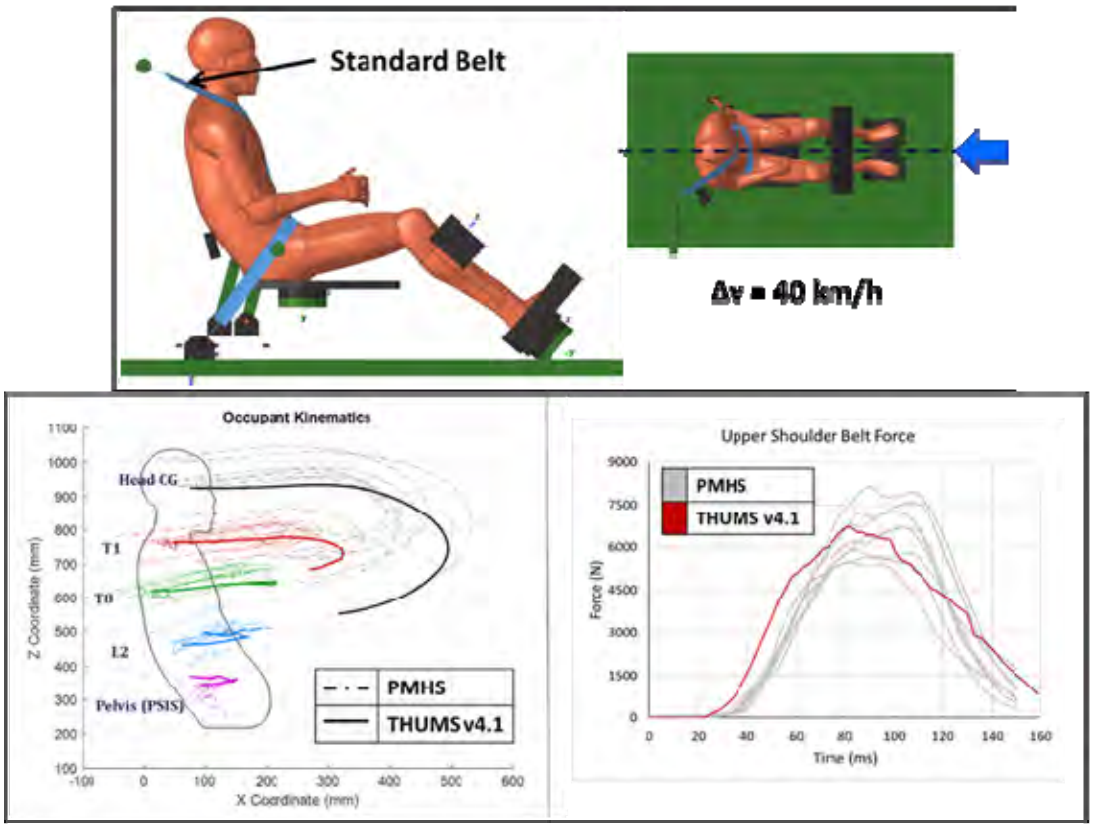

Fig. A13: *Gold-Standard 1* sled setup of [25]. Restraints included a 3-point standard (not force limited) belt and a rigid, closely-placed knee bolster.

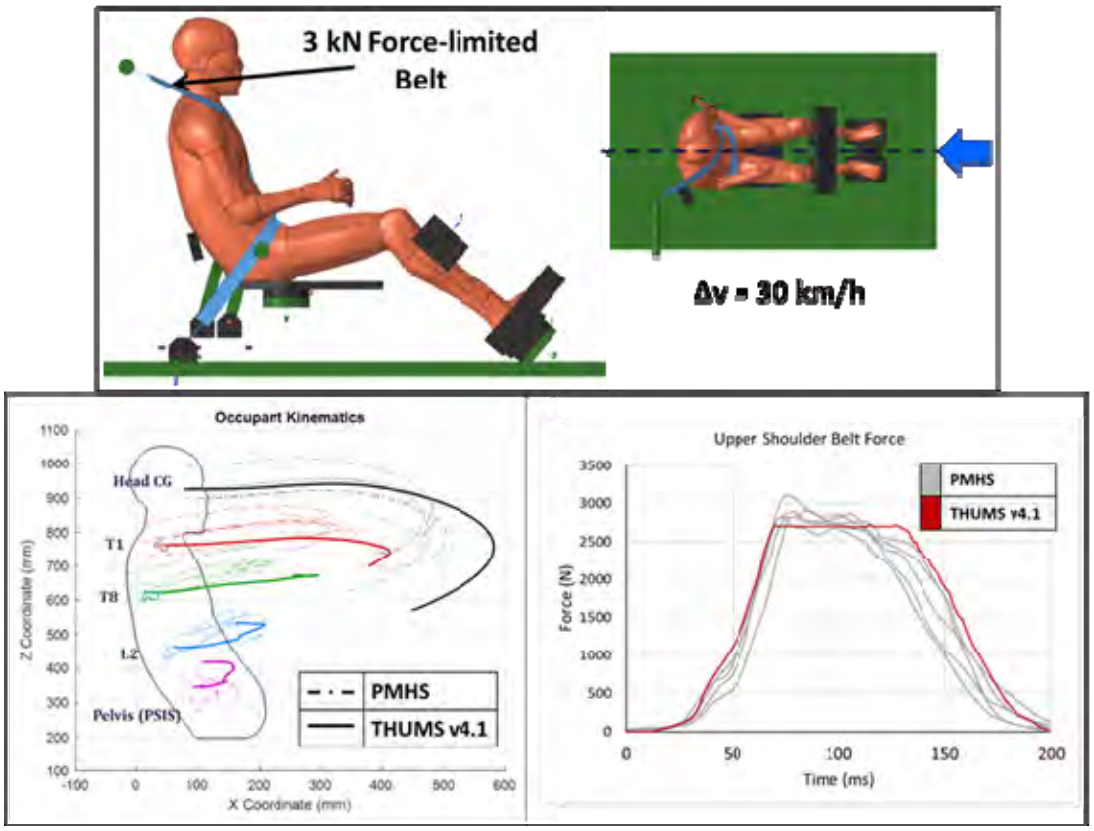

Fig. A14. *Gold-Standard 2* sled setup of [26]. Restraints included a force-limited 3-point belt and a rigid, closely-placed knee bolster.

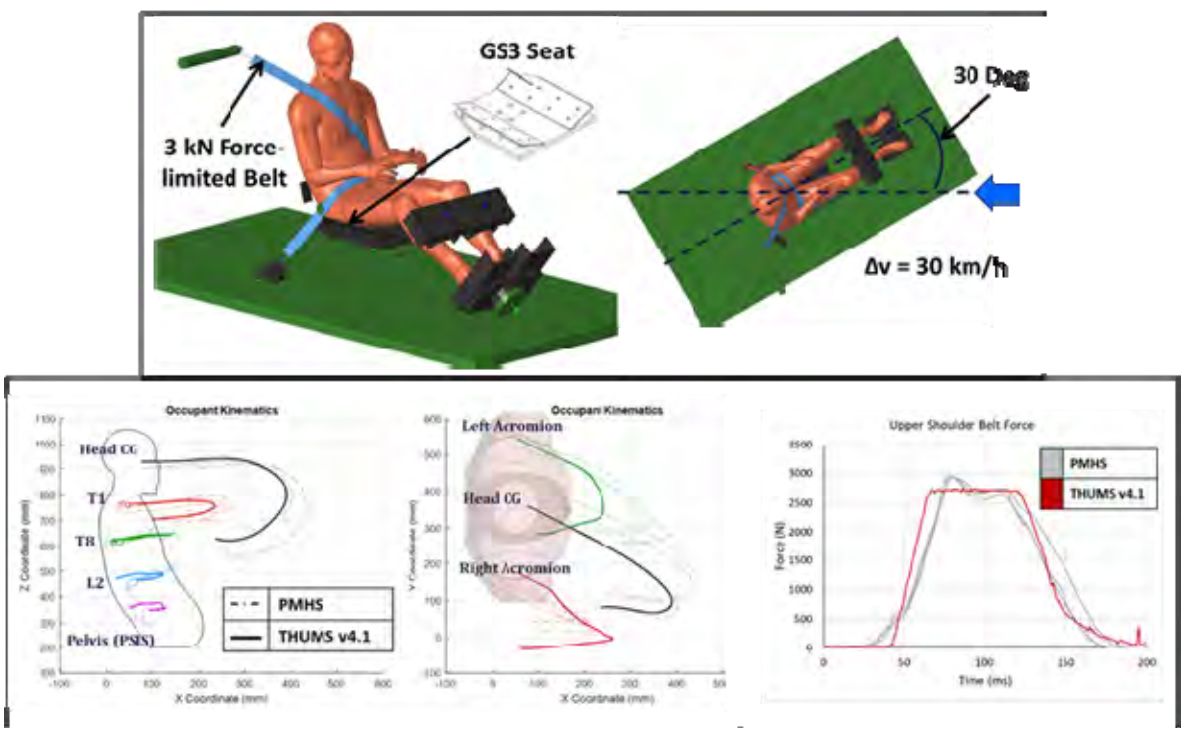

Fig. A15 *Gold-Standard 3* sled setup of [26]. Restraints included a force-limited 3-point belt and a rigid, closely-placed knee bolster.

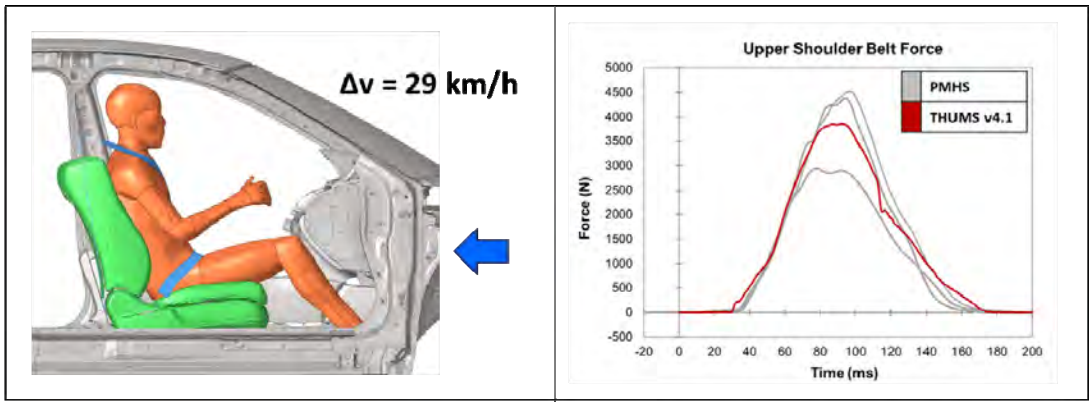

Fig. A16. Low-speed sled setup of [29]. Restraints included a knee bolster and standard (not force limited or pretensioned) 3-point belt.

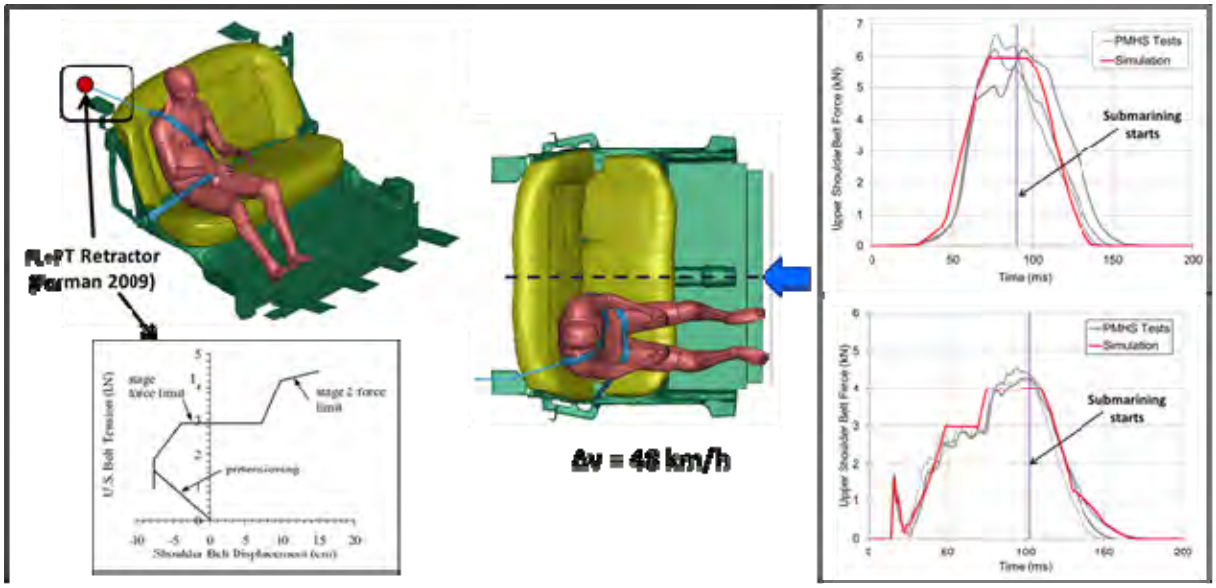

Fig. A17. Rear seat sled setup of [28] and [27]. The tests of [28] used a standard (not force limited or pretensioned) 3-point belt (top-right force plot). The tests of [27] used a 3-point belt with a retractor pretensioner and progressive force limiter (bottom-right force plot, and inset force-displacement plot).

Appendix B:

TABLE B I
PMHS DETAILS AND INJURY INFORMATION FOR ALL TESTS REFERENCED IN THIS STUDY

Loadcase	PMHS_ID	Test_ID	Age	Sex	Height (cm)	Weight (kg)	Total Rib Fractures	3+ Rib Fractures	7+ Rib Fractures
01_[15]	119FM	218	69	M	178.3	65	11	1	1
	121FM	219	66	M	185.5	68.2	6	1	0
	123FM	220	58	M	173.7	72.3	7	1	1
02_ [16]	1	1	72	M	170	82	5	1	0
	2	2	81	M	175	63	4	1	0
	3	3	84	M	168	68	0	0	0
	4	4	86	M	170	56	2	0	0
	5	5	62	M	174	61	3	1	0
	6	6	70	M	169	91	4	1	0
	7	7	68	M	178	83	11	1	1
03_ [17]	28800	GI5	65	F	164	61	13	1	1
	29084	GI10	64	M	180	65	20	1	1
	29115	GI11	74	M	168	75	16	1	1
04_ [18]	2000-FRM-135	Cad1	63	M	172.6	69.1	3	1	0
	2002-FRM-159	Cad2	66	M	166.5	65.9	2	0	0
	2001-FRM-149	Cad3	40	M	158.3	43.1	1	0	0
	2002-FRM-161	Cad4	61	M	181.7	65.8	16	1	1
05_ [14]	11FF	60	60	F	160	58.9	11	1	1
	12FF	61	67	F	162.5	62.6	24	1	1
	13FM	65	81	M	167.6	76.2	21	1	1
	14FF	66	76	F	157.5	57.6	7	1	1
	15FM	69	80	M	165.1	53	13	1	1
	18FM	76	78	M	175.3	65.7	16	1	1
	19FM	77	19	M	NA	65.7	1	0	0
	20FM	79	29	M	180.3	56.7	0	0	0
	21FF	82	45	F	172.7	68.5	19	1	1
	22FM	83	72	M	182.9	74.8	17	1	1
	23FF	85	58	F	162.5	61.2	23	1	1
	24FM	86	65	M	182.9	81.6	6	1	0
	25FM	87	65	M	167.6	54.4	18	1	1
	26FM	88	75	M	172.7	63.5	0	0	0
	28FM	90	54	M	182.9	68	0	0	0
	30FF	92	52	F	156	40.8	3	1	0
	31FM	93	51	M	183	74.8	15	1	1
	32FM	94	75	M	171	54.4	21	1	1
	34FM	96	64	M	178	59	13	1	1
	36FM	99	52	M	183	74.8	7	1	1
	37FM	104	48	M	179	73.9	10	1	1
	42FM	171	61	M	183	54.4	0	0	0
	43FM	172	59	M	178	54.4	4	1	0
	45FM	177	64	M	181	64	11	1	1
	46FM	178	46	M	178	94.8	0	0	0
	48FM	182	69	M	170	64.4	0	0	0
	50FM	186	66	M	181	59.9	13	1	1

	51FM	187	60	M	185	82.1	0	0	0
	52FM	188	65	M	175	51.7	12	1	1
	53FM	189	75	M	174	77.1	3	1	0
	54FF	190	49	F	163	37.2	7	1	1
	55FF	191	46	F	177	81.2	8	1	1
	56FM	192	65	M	177	73.9	3	1	0
	58FM	196	68	M	179	68.9	4	1	0
	60FM	200	66	M	180	79.4	9	1	1
	62FM	202	76	M	174	50.3	10	1	1
	63FM	203	53	M	183	88	5	1	0
	64FM	204	72	M	163	63	6	1	0
06_ [19]	147	Cadve42	63	F	161	45	0	0	0
	145	Cadve62	54	M	192	87.7	0	0	0
	145	Cadve64	54	M	192	87.7	6	1	0
	155	Cadve67	71	F	166	54.4	0	0	0
	170	Cadve87	75	M	178	65	0	0	0
	173	Cadve103	67	F	162	57.2	0	0	0
	178	Cadve127	73	M	182	80.7	0	0	0
	177	Cadve146	79	F	161	47.6	0	0	0
	177	Cadve149	79	F	161	47.6	24	1	1
	176	Cadve152	85	F	157	58.2	0	0	0
	182	Cadve171	80	F	157	65.3	0	0	0
	157	Cadve179	55	F	168	74.4	0	0	0
	186	Cadve197	58	F	178	61.2	0	0	0
	186	Cadve201	58	F	178	61.2	8	1	1
	188	Cadve203	71	M	173	85.3	0	0	0
	187	Cadve217	54	M	178	112.7	1	0	0
	190	Cadve230	79	M	173	73.5	0	0	0
	189	Cadve248	79	M	159	56.7	0	0	0
07_ [19]	147	Cadve45	63	F	161	45	0	0	0
	145	Cadve57	54	M	192	87.7	0	0	0
	155	Cadve73	71	F	166	54.4	0	0	0
	170	Cadve96	75	M	178	65	0	0	0
	170	Cadve98	75	M	178	65	11	1	1
	173	Cadve100	67	F	162	57.2	0	0	0
	178	Cadve120	73	M	182	80.7	0	0	0
	177	Cadve143	79	F	161	47.6	0	0	0
	176	Cadve155	85	F	157	58.2	0	0	0
	182	Cadve167	80	F	157	65.3	0	0	0
	157	Cadve176	55	F	168	74.4	0	0	0
	186	Cadve195	58	F	178	61.2	0	0	0
	188	Cadve207	71	M	173	85.3	0	0	0
	187	Cadve221	54	M	178	112.7	0	0	0
	190	Cadve232	79	M	173	73.5	0	0	0
	189	Cadve250	79	M	159	56.7	0	0	0
08_ [19]	147	Cadve50	63	F	161	45	1	0	0
	145	Cadve54	54	M	192	87.7	0	0	0
	155	Cadve69	71	F	166	54.4	1	0	0
	170	Cadve93	75	M	178	65	1	0	0

	173	Cadve105	67	F	162	57.2	0	0	0
	178	Cadve124	73	M	182	80.7	1	0	0
	177	Cadve139	79	F	161	47.6	1	0	0
	176	Cadve159	85	F	157	58.2	0	0	0
	176	Cadve161	85	F	157	58.2	8	1	1
	182	Cadve163	80	F	157	65.3	0	0	0
	182	Cadve174	80	F	157	65.3	22	1	1
	157	Cadve182	55	F	168	74.4	1	0	0
	186	Cadve192	58	F	178	61.2	1	0	0
	188	Cadve209	71	M	173	85.3	1	0	0
	187	Cadve225	54	M	178	112.7	0	0	0
	187	Cadve228	54	M	178	112.7	1	0	0
	190	Cadve234	79	M	173	73.5	0	0	0
	189	Cadve246	79	M	159	56.7	0	0	0
09_ [19]	155	Cadve71	71	F	166	54.4	0	0	0
	170	Cadve90	75	M	178	65	0	0	0
	173	Cadve107	67	F	162	57.2	0	0	0
	178	Cadve122	73	M	182	80.7	1	0	0
	177	Cadve141	79	F	161	47.6	0	0	0
	176	Cadve157	85	F	157	58.2	0	0	0
	182	Cadve165	80	F	157	65.3	0	0	0
	157	Cadve184	55	F	168	74.4	0	0	0
	157	Cadve188	55	F	168	74.4	27	1	1
	186	Cadve190	58	F	178	61.2	0	0	0
	188	Cadve211	71	M	173	85.3	0	0	0
	187	Cadve223	54	M	178	112.7	0	0	0
	190	Cadve236	79	M	173	73.5	0	0	0
	190	Cadve240	79	M	173	73.5	12	1	1
	189	Cadve242	79	M	159	56.7	0	0	0
10_ [22]	1	01Male	65	M	183	76.8	14	1	1
	2	02Female	69	F	155	50.9	8	1	1
11_ [21]	412	12	62	M	175	68	0	0	0
	412	13	62	M	175	68	0	0	0
	413	22	54	M	175	68	0	0	0
	413	23	54	M	175	68	0	0	0
	419	33	31	M	193	90	0	0	0
	419	34	31	M	193	90	0	0	0
12_ [20]	207	cadve205	67	F	160	49.9	0	0	0
	207	cadve206	67	F	160	49.9	0	0	0
	207	cadve207	67	F	160	49.9	0	0	0
	207	cadve208	67	F	160	49.9	0	0	0
	207	cadve209	67	F	160	49.9	0	0	0
	207	cadve210	67	F	160	49.9	0	0	0
	207	cadve212	67	F	160	49.9	8	1	1
	194	cadve217	38	F	170	94.8	0	0	0
	194	cadve218	38	F	170	94.8	0	0	0
	194	cadve219	38	F	170	94.8	0	0	0
	194	cadve220	38	F	170	94.8	0	0	0
	194	cadve221	38	F	170	94.8	0	0	0

	194	cadve222	38	F	170	94.8	0	0	0
	194	cadve223	38	F	170	94.8	0	0	0
	194	cadve225	38	F	170	94.8	0	0	0
	195	cadve227	67	F	173	58.9	0	0	0
	195	cadve229	67	F	173	58.9	0	0	0
	195	cadve230	67	F	173	58.9	0	0	0
	195	cadve231	67	F	173	58.9	0	0	0
	195	cadve232	67	F	173	58.9	0	0	0
	195	cadve233	67	F	173	58.9	0	0	0
	195	cadve234	67	F	173	58.9	0	0	0
	195	cadve238	67	F	173	58.9	21	1	1
13_ [23, 24]	THC11	thc11	47	F	170	92.5	8	1	1
	THC12	thc12	17	F	164	58.5	0	0	0
	THC13	thc13	86	F	160	43	2	0	0
	THC14	thc14	69	M	173	82	17	1	1
	THC15	thc15	60	M	177	69	3	1	0
	THC16	thc16	59	M	170	62	4	1	0
	THC17	thc17	71	M	177	75	7	1	1
	THC18	thc18	67	M	174	47	6	1	0
	THC19	thc19	83	F	155	43	4	1	0
	THC20	thc20	70	M	160	63	18	1	1
	THC62	thc62	72	M	183	53	4	1	0
	THC65	thc65	71	M	170	41	10	1	1
	THC69	thc69	40	M	183	56	1	0	0
	THC75	thc75	60	M	160	44.5	6	1	0
	THC77	thc77	64	F	164	49.5	6	1	0
	THC79	thc79	43	M	186	54	3	1	0
	THC93	thc93	63	M	176	56	10	1	1
Gold Standard 1 [25]	411	1294	76	M	178	70	8	1	1
	403	1295	47	M	177	68	29	1	1
	425	1358	54	M	177	79	16	1	1
	426	1359	49	M	184	76	11	1	1
	428	1360	57	M	175	64	6	1	0
	443	1378	72	M	184	81	10	1	1
	433	1379	40	M	179	88	11	1	1
	441	1380	37	M	180	78	2	0	0
Gold Standard 2 [26]	494	UVAS028	59	M	178	68	0	0	0
	492	UVAS029	66	M	179	70	0	0	0
	674	UVAS0302	67	M	177	68	4	1	0
	736	UVAS0303	67	M	173	68	8	1	1
	695	UVAS0304	74	M	183	70	0	0	0
Gold Standard 3 [26]	632	UVAS0313	69	M	173	69	7	1	1
	750	UVAS0314	66	M	171.5	76	8	1	1
	767	UVAS0315	67	M	176.5	64	0	0	0
Rear Seat (Forman 2009) [27]	1	1386	67	M	175	69	12	1	1
	2	1387	69	M	171	67	3	1	0
	3	1389	72	M	183	72	17	1	1
Rear Seat (Michaelson	1	1262	51	M	175	54.9	14	1	1
	2	1263	57	F	165	108.9	30	1	1

2008) [28]	3	1264	57	M	179	59	14	1	1
Low Speed Frontal [29]	322	1094	49	M	178	58.1	0	0	0
	327	1096	39	M	184	79.4	0	0	0
	323	1095	44	M	172	77.1	0	0	0

Appendix C:

TABLE C I
IMPACTOR MASSES AND VELOCITIES FOR IMPACTOR CASES

Loadcase	PMHS_ID	Test_ID	Test Impactor Mass (kg)	Test Impactor Initial Velocity (m/s)	Scaled impactor mass for THUMS v4.1 (kg)
01_[15]	119FM	218	4.25	13.4	5.03
	121FM	219	4.25	13.4	4.80
	123FM	220	4.25	13.4	4.53
02_ [16]	1	1	23.5	4.3	22.07
	2	2	23.5	4.3	28.72
	3	3	23.5	4.3	26.61
	4	4	23.5	4.3	32.31
	5	5	23.5	4.3	29.66
	6	6	23.5	4.3	19.88
	7	7	23.5	4.3	21.80
03_ [17]	28800	GI5	48	6	60.59
	29084	GI10	48	8.9	56.86
	29115	GI11	48	6.2	49.28
04_ [18]	2000-FRM-135	Cad1	64	4	71.32
	2002-FRM-159	Cad2	64	4	74.78
	2001-FRM-149	Cad3	64	4	114.34
	2002-FRM-161	Cad4	64	4	74.89
05_ [14]	11FF	60	19.5	6.3	25.49
	12FF	61	22.8	7.2	28.04
	13FM	65	22.8	7.4	23.04
	14FF	66	22.8	7.3	30.48
	15FM	69	23.6	6.9	34.29
	18FM	76	23.6	6.7	27.66
	19FM	77	23.6	6.7	27.66
	20FM	79	23.6	6.7	32.05
	21FF	82	23.6	6.8	26.53
	22FM	83	23.6	6.7	24.29
	23FF	85	19.5	7.7	24.53
	24FM	86	22.8	9.6	21.51
	25FM	87	5.5	13.8	7.78
	26FM	88	1.8	11.1	2.18
	28FM	90	1.6	14.5	1.81
	30FF	92	15.9	13.23	30.01
	31FM	93	23.04	10.19	23.72
	32FM	94	22.86	9.92	32.36
	34FM	96	18.96	8.23	24.74
	36FM	99	18.96	7.2	19.52
	37FM	104	22.86	9.83	23.82
	42FM	171	22.86	4.87	32.36
	43FM	172	22.86	4.83	32.36
	45FM	177	23	5.05	27.67
	46FM	178	19.28	7.33	15.66
	48FM	182	10.43	7.06	12.47

	50FM	186	10.43	7.29	13.41
	51FM	187	10.43	6.66	9.78
	52FM	188	10.43	7.2	15.53
	53FM	189	22.95	5.23	22.92
	54FF	190	19.55	6.71	40.47
	55FF	191	19.55	9.92	18.54
	56FM	192	10.43	6.93	10.87
	58FM	196	10.43	6.75	11.66
	60FM	200	22.95	4.34	22.26
	62FM	202	9.98	6.93	15.28
	63FM	203	23	6.93	20.13
	64FM	204	23	6.93	28.11

Appendix D

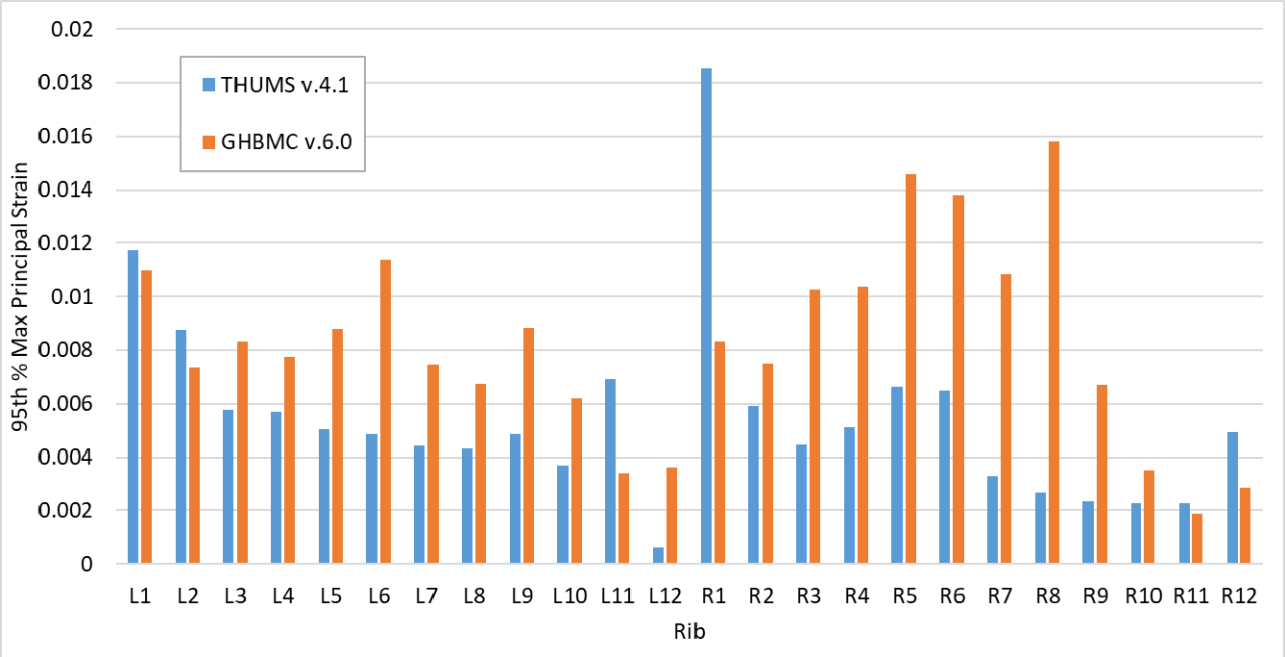

Fig. D1. 95th Percentile Maximum Principal Strains Observed in the THUMS v.4.1 and GHBMC v.6.0 in the 56 km/h Frontal Barrier Simulations with the 2014 Honda Accord FE Environment.